Towards An Adaptive-Compliance Aerial Manipulator for Contact-Based Interaction

Salua Hamaza[1*], Ioannis Georgilas[2], Thomas Richardson[1,3]

***Abstract*— As roles for unmanned aerial vehicles (UAVs) continue to diversify, the ability to sense and interact closely with the environment becomes increasingly important. Within this paper we report on the initial flight tests of a novel adaptively compliant actuator which will allow a UAV to carry out such tasks as the "pick and placement" of remote sensors, structural testing and contact-based inspection. Three key results are discussed and presented; the ability to physically apply forces with the UAV through the use of an active compliant manipulator; the ability to tailor these forces through tuning of the manipulator controller gains; and the ability to apply a rapid series of physical pulses in order to excite remotely placed sensors, e.g. vibration sensors. A series of over sixty flight tests have been used to generate initial results which clearly demonstrate the potential of this new type of compliant aerial actuator.**

I. Introduction

A common problem faced nowadays relates to ageing of existing infrastructure. To underpin this problem, periodic maintenance and inspection of such large-scale systems is increasingly in demand, often requiring human operators to intervene in hard-to-reach locations, involving hazards, high risks and insurance costs. Real-time monitoring of the infrastructure is also a key challenge for companies that wish to reduce the costly on-site intervention.

Aerial manipulators, i.e. Unmanned Aerial Vehicles (UAVs) equipped with a manipulation system, are aerial systems capable of interacting with the environment that can come to aid in contact-based inspection and repair tasks. Advances in sensing technologies have allowed UAVs to perform on-call contact-less inspection, however no long-term solution is yet in place to address the challenge of real-time monitoring. Aerial manipulators capable of positioning small objects in hard-to-reach locations, e.g. sensors, can address inspection of infrastructure in real-time. Some examples of this are the placement of ohmmeters to detect faults on wind turbine blades, smoke detectors in forests for fire prevention, pressure sensors on dams, strain gauges on bridges, etc.

So far, research in the field of aerial physical interaction has focused on interaction with the environment for performing tasks such as non-destructive testing [1] or contact operations conducted in quasi-static conditions [2]–[4]. The challenge of exerting forces in the environment has been addressed multiple times in the state-of-the-art and some key results show the application of up to 5 N in quasi-static conditions [5], [6]. In [7] a simple 1-DoF manipulator is used to perform aerial bridge inspection. The desired force at the end-effector is achieved by converting the rotors' horizontal thrust into the demanded interaction force, by increasing the pitch angle of the vehicle whilst in contact.

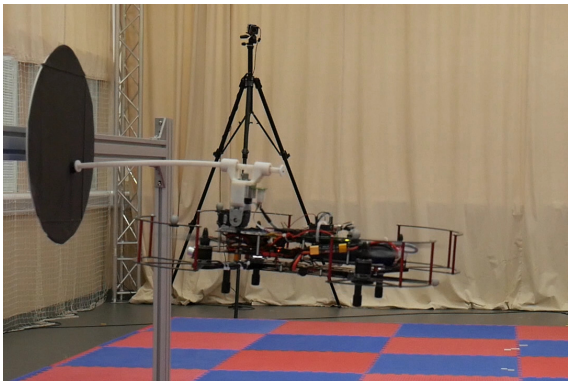

Fig. 1: A multirotor equipped with an adaptively compliant manipulator interacting with a vertical surface.

The benefits of having compliance as part of the aerial manipulation system have been demonstrated, both in hardware and software. In [8], [9] a passive compliant manipulator comprising a spring-lock mechanism is used for impact absorption and stable contact with wall. In [10] a bio-inspired lightweight arm is presented, where active compliance allows for payload estimation and compensation in the altitude control. In [11] a compliant finger module is added to the existing manipulator for soft collision detection and obstacle localization. In [12] a variable-compliance aerial manipulator is used to tailor different demanded forces at the end-effector during interaction with a wall. In [13] a collision-resilient flying robot is encapsulated within a protective case which enables impact absorption thanks to the material properties. Similarly, in [14] a passive gimbal mounted on an external structure transforms the UAV linear kinetic energy generated from an impact into rotational energy of the surrounding structure, preserving the position of the UAV Centre of Gravity (CoG).

With regards to compliance implemented in software, several contributions in the state-of-the-art demonstrate how compliant control aids force estimation and motion feedback at the end-effector, improving stable contact during an interaction [15]–[18]. Other research considers the negative influence of moving parts on the aircraft stability, which affect both the attitude and altitude dynamics. Hence, changes to the UAV's CoG should be minimised to improve flight stability and endurance [19]–[21].

This work was supported by the EPSRC Centre for Doctoral Training in Future Autonomous and Robotic Systems (FARSCOPE).

[1] Bristol Robotics Laboratory, University of Bristol and University of the West of England, Bristol, UK. *s.hamaza@bristol.ac.uk

[2]Dept. of Mechanical Engineering, University of Bath, Bath, UK.

[3]Dept. of Aerospace Engineering, University of Bristol, Bristol, UK.

This paper builds upon what has been demonstrated in previous works to address the challenges of aerial dynamic interaction, and proposes a novel manipulator design that features actively-variable compliance. Two scenarios are envisioned for the proposed aerial system: the placement of small sensors for real-time monitoring and hazard prevention; and the excitation of sensors through a series of physical pulses for inspection, maintenance or cleaning purposes. The case study for these operations is the interaction against flat surfaces such as those found on dams, power-plant chimneys, bridges etc.

Thus, the two main contributions presented in this paper are the design of a bespoke manipulator able to exert different demanded forces thorough the tuning of its variable-compliance; and the ability to shape the loads applied, e.g. a single pulse for longer periods of time, or a rapid series of shorter pulses.

II. Aerial Manipulator Dynamics

In this section, we present a brief description of the system model. We represent the aerial manipulator as a multi-rotor carrying an external load. The study of the dynamics of this type of system are presented in the literature in several works [3], [22]–[25], the basis of which we use here to highlight the key variables that will drive the design of a bespoke manipulator.

Aerial Vehicle Model

We consider a generic aerial system with n-rotors as a 6 DoFs rigid body. We identify two coordinate frames referring to the ground-truth, namely world frame $\mathcal{W}$, and the body-fixed frame $\mathcal{A}$ centred in the vehicle CoG. The pose of the moving body with respect to the world frame is described by the vector $\mathbf{p} = [\zeta_x \ \zeta_y \ \zeta_z \ \phi_R \ \theta_P \ \psi_Y]^T$ comprising of translational and rotational terms. The equation of motion of the system is:

$$\mathbf{M}\ddot{\mathbf{p}} + \mathbf{C}(\mathbf{p}, \dot{\mathbf{p}})\dot{\mathbf{p}} + \mathbf{G}(\mathbf{p}) = \tau + \tau_{\mathbf{man}} \tag{1}$$

where $\mathbf{M}$ is the mass matrix with all inertial terms of the system, $\mathbf{C}$ is a skew-symmetric matrix with centripetal and Coriolis terms, $\mathbf{G}$ represents the gravitational terms acting on the system. On the right side, τ represents the output torque and thrust force generated by the vehicle's rotors; $\tau_{\mathbf{man}} = [\mathbf{F_m} \ \mathbf{M_m}]^T$ is the vector of external forces and moments induced on the vehicle by the manipulator.

Manipulator Model

We are interested to know how the terms $\mathbf{F_m}$ and $\mathbf{T_m}$ affect the aerial vehicle's dynamics during interaction. We will start by modeling the manipulator as a suspended load on the vehicle. We define a new coordinate frame $\mathcal{M}$ centred in the manipulator's CoG. The position of the manipulator's CoG, namely the origin of frame $\mathcal{M}$, varies over time as the manipulator moves to perform a task, and this motion is independent of the aircraft motion. As seen before, we define the pose of the manipulator's CoG with respect to

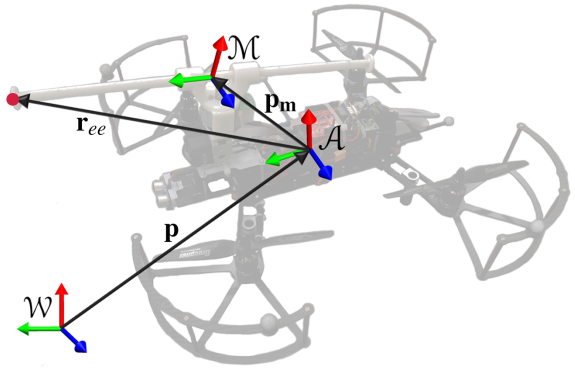

Fig. 2: Aerial manipulator sketch and coordinate frames.

frame $\mathcal{A}$ with vector $\mathbf{p_m} = [\zeta_{mx} \ \zeta_{my} \ \zeta_{mz} \ \phi_{mR} \ \theta_{mP} \ \psi_{mY}]^T$. The manipulator's equation of motion is:

$$\mathbf{M}\ddot{\mathbf{p}}_\mathbf{m} + \mathbf{C}(\mathbf{p_m}, \dot{\mathbf{p}}_\mathbf{m})\dot{\mathbf{p}}_\mathbf{m} + \mathbf{G}(\mathbf{p_m}) = \sigma_{\mathbf{ext}} \tag{2}$$

where $\mathbf{M}$ is the mass matrix of the system, $\mathbf{C}$ is the damping matrix with centripetal and Coriolis terms and $\mathbf{G}$ is the matrix describing the gravitational terms. For the equilibrium, this equates to the sum of all external forces and moments acting on the manipulator σ_{ext}, for example the external actions due to interaction. It is to be noted that eq. (2) solely describes the manipulator dynamics and does not consider the dynamic effects of the aerial vehicle (see eq. (1)).

We now define vector $\mathbf{r}_{ee} = [x_{ee} \ y_{ee} \ z_{ee}]^T$ that links the origin of frame $\mathcal{A}$ to the tip of the end-effector, as illustrated in fig. 2. The external forces and moments acting on the vehicle caused by the interaction of the end-effector with the environment, expressed in frame $\mathcal{A}$ are:

$$\sigma_{ext} = \begin{bmatrix} \mathbf{R}_M^A \ \mathbf{F}_{int} \\ \mathbf{R}_M^A \ \mathbf{M}_{int} + \mathbf{r}_{ee} \times \mathbf{R}_M^A \ \mathbf{F}_{int} \end{bmatrix} \tag{3}$$

where $\mathbf{F}_{int}$ and $\mathbf{M}_{int}$ represent the interaction force and moment respectively, and $\mathbf{R}_M^A$ is the rotation matrix from frame $\mathcal{A}$ to frame $\mathcal{M}$.

To be able to minimise the disturbances caused by the interaction to the aerial vehicle we will act upon terms $\mathbf{F}_{int}$ and $\mathbf{M}_{int}$ and $\mathbf{r}_{ee}$. Hence, they become the three key drivers for the design a manipulation system that:

- is able to absorb/filter the undesired forces $\mathbf{F}_{int}$ exerted at the end-effector and mitigate the propagation of those to the aircraft with the use of actively-variable compliance.
- has a small-sized end-effector in order to reduce the moment $\mathbf{M}_{int}$ transferred during interaction.
- allows to move the location of the end-effector irrespective of the aircraft, so to reduce vector $\mathbf{r}_{ee}$.

III. Manipulator Design

Based on the previous section conclusions, we propose a novel lightweight manipulator featuring active variable compliance for mitigating the interaction forces $\mathbf{F}_{int}$ over the aircraft. The bespoke manipulation system is designed to perform tasks such as the placement of sensors, probing and tapping; and comprises 2 DoF to allow independent motion of the end-effector irrespective of the vehicle.

A. Manipulator Mechanical Design

The manipulation system consists of two active DoFs that provide independent translation and pitching of the end-effector. The rotational DoF is actuated by a servo motor, whilst the translational DoF is comprised of a rack-and-pinion system driven by a DC brushless motor. The rack-and-pinion transmission, illustrated in fig. 3, can behave as an adaptive-spring/adaptive-damper system thanks to a variable-gain PID control embedded on the DC motor. This allows to actively adjust the forces $\mathbf{F}_{int}$ exerted/absorbed by the end-effector. To minimise the effect of the moment $\mathbf{M}_{int}$, the size of the end-effector is kept small. For the purpose of initial validation of the proposed manipulator, the design of a gripper is omitted, hence we will consider the end-effector to be the tip of the rack itself. Lastly, the manipulator configuration is such that the inertias are minimised, i.e. the design is compact, and that the flight time is increased, i.e. no moving masses are present except for the sliding rack ($\approx$80 gr).

B. Manipulator Controller

The actuated rack-and-pinion system replicates an adaptive torsional spring behaviour. The inspiration for this design comes from the working principle of flat spiral springs which resist the unwinding of the coil through the spring material properties. The DC motor recreates this behaviour through a variable-gain PID controller: as the rack diverges from a set position due to external forces, the torque output of the motor increases in order to counterbalance this action. As a result, the rack is stiffened in the opposite direction.

The use of PID control to achieve compliance at the end-effector is based on the analogy between a PID controller and spring-damper systems: the proportional gain K_p provides the rack with a spring-like behaviour, similar to the spring coefficient, whilst K_d controls the damping. A Ziegler Nichols [26] approach was used in order to tune the manipulator PID gains, as illustrated in table I. Variables K_u and T_u represent the ultimate gain and the oscillation period respectively, for which stable and consistent oscillations occur.

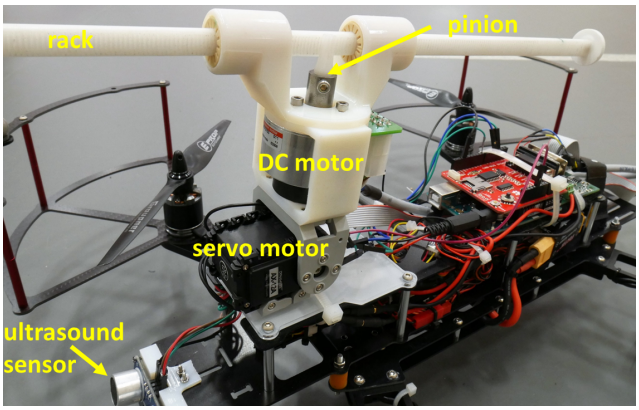

Fig. 3: Manipulator setup: a translational DoF is driven by a rack-and-pinion system actuated by a DC motor. Linear motion of the rack is bidirectional and controlled by a variable-gain PID controller. A servo motor provides independent pitching of the rack. An ultrasound sensor feeds range information to the PID control.

K_u	T_u	$K_p = 0.6\ K_u$	K_i	K_d
8	0.045	4.8	214.765	0.027

TABLE I: Ziegler-Nichols parameters used for tuning the PID control gains.

To change the demanded force at the end-effector and thus validate the adaptive behaviour, we vary the control system gains for the actuated rack. It is assumed that lower proportional gains generate more compliant behaviours of the rack and a less aggressive response to displacement and force exertion.

Moreover, by changing the desired output of the PID control we are able to shape the load curve and therefore perform different tasks. For example, in a probing operation a setpoint is computed such that the rack protrudes out and remains in the proximity of a surface. For other tasks, such as tapping, the rack protrudes out to establish contact with a wall and then periodically taps onto it. In case the desired operation is the placement of an object, a demanded setpoint is computed *beyond* the wall location inducing the end-effector to reach the wall and further increase the force in an attempt to satisfy the control demand.

IV. Flight Experiments

In this section we present the initial flight tests that have been carried out in order to validate the proposed aerial manipulator. Over 60 airborne experiments were conducted to demonstrate both the effect of adaptive compliance and the ability to perform different tasks, such as pushing against, or tapping a surface.

A. Experimental Setup

The platform chosen for the experimental validation is the quadcopter Lumenier QAV400® (950 gr) powered by a 4s 4000mAh battery (425 gr). The manipulator overall mass is about 450 gr; the aircraft all-up weight is 1.85 kg. Off-the-shelf Delrin® parts are selected for the rack and pinion; custom linear bearings and a 3D printed case house the rack-pinion mechanism. A direct drive Maxon® motor EC 45 flat (50 Watt, 780 mNm stall torque, 150 gr, Hall sensor and encoder) actuates the translational DoF. This motor was chosen for its ability to output high torques. A Dynamixel AX-12A servo motor drives the pitch of the rack and a HC-SR04 ultrasound sensor is mounted at the front of the aircraft as a separate input to the PID control. The PID control is implemented on an on-board computer with CAN bus and data logging capabilities. A 6-axis Force/Torque sensor (FTSens, IIT, Italy) is mounted on the wall where contact takes place, providing ground truth measurements of the interaction force. All flight experiments are conducted in a VICON motion capture system in order to acquire the UAV's ground truth measurements.

B. Pushing Task

The first scenario addresses the application of force on a vertical wall. Four different gains have been selected to validate the adaptive compliance behaviour of the manipulator, with proportional gains at 10%, 20%, 50%, and 60%

	K_p = 0.8	K_p = 1.6	K_p = 4	K_p = 4.8
$\mu_{roll} \pm \sigma_{roll}$	0.36 ± 0.81	0.29 ± 1.00	0.31 ± 1.09	0.72 ± 1.30
peak amplitude$_{roll}$	2.25	2.39	2.47	2.46
$\mu_{pitch} \pm \sigma_{pitch}$	0.70 ± 3.45	0.73 ± 3.76	0.75 ± 4.16	0.73 ± 4.24
peak amplitude$_{pitch}$	9.37	10.63	11.24	17.30
$\mu_{yaw} \pm \sigma_{yaw}$	-0.57 ± 1.77	-0.05 ± 1.95	-0.64 ± 2.06	-0.84 ± 2.89
peak amplitude$_{yaw}$	0.09	0.17	1.16	0.59

TABLE II: Mean value μ [deg], standard deviation σ [deg] and peak amplitude [deg] of the UAV angular states (roll-pitch-yaw) measured by the VICON tracking system and averaged over a minimum of 10 flights for each K_p.

of the ultimate value K_u; respectively K_p = 0.8, 1.6, 4 and 4.8. For each of these gains, at least 10 flights have been conducted. All gains tested are within the limit found through Ziegler-Nichols ($K_p \leq 4.8$, see table I). Over 50 flights in total demonstrate the *pushing* task.

Each experiment is laid out as follows: the aircraft flies through a series of way-points allowing it to reach the target location at a constant speed of 0.25 m/sec and repeatably perform the interaction task. The dataset generated at each flight can be segmented as follows: *moving towards the target, interaction task, recovery/settling period, homing*. For every flight the effects of interaction on the UAV response are measured through the CoG position *x-y-z* and orientation *roll-pitch-yaw* angles, tracked by the VICON motion capture system. The forces exerted on the wall are also measured through the Force/Torque sensor.

Table II shows the effect of adaptive compliance on the UAV angular dynamics. The mean value μ, standard deviation σ and peak amplitude of the UAV *roll-pitch-yaw* angles are presented, averaged over all flights conducted with the same K_p. To extrapolate the trend of the angular dynamics during interaction we compute μ and σ considering the *interaction* and *recovery/settling period* segments in the dataset, discarding the *homing* and *target approaching* parts.

It is clear that, by increasing the stiffness of the manipulator, i.e. higher proportional gains in the PID control, the standard deviation σ increases indicating that higher disturbances propagate to the aircraft. In particular, the pitch state is the one most affected during the interaction (see σ_{pitch} and peak amplitude$_{pitch}$ in table II). A comparison between the peak amplitude$_{pitch}$ in the first and last column of the table shows an outcome that is almost doubled in magnitude, leading to a peak amplitude up to 17 degrees. Figure 5 provides a side-view on the aircraft interacting with the wall. This time-lapse sequence was recorded during a single flight with K_p = 4.8 and clearly shows the oscillatory behaviour in pitch of the vehicle after the task has been completed.

Table II also provides information on disturbances about the x-z axes, namely changes in *roll-yaw* angles. We can infer that a higher compliance benefits the angular dynamics of the UAV in different measures: despite an increase in the σ_{yaw} of about $+1$ degree, the peak amplitude of both roll and yaw angles are consistently low throughout the table.

In fig. 4 the variation in pitch angle over time is displayed for each K_p tested. In each sub-figure, a sample of the pitch data captured during a single flight has been plotted against the averaged mean μ_{pitch} and standard deviation σ_{pitch} from table II to provide a visual cue on the increase of σ_{pitch} (width of the greyed bands) over higher gains. The peak amplitude of each sample flight also increases accordingly.

A comparison of the forces exerted by the end-effector during interaction is illustrated in fig. 6. It is demonstrated that more compliant configurations generate lower forces

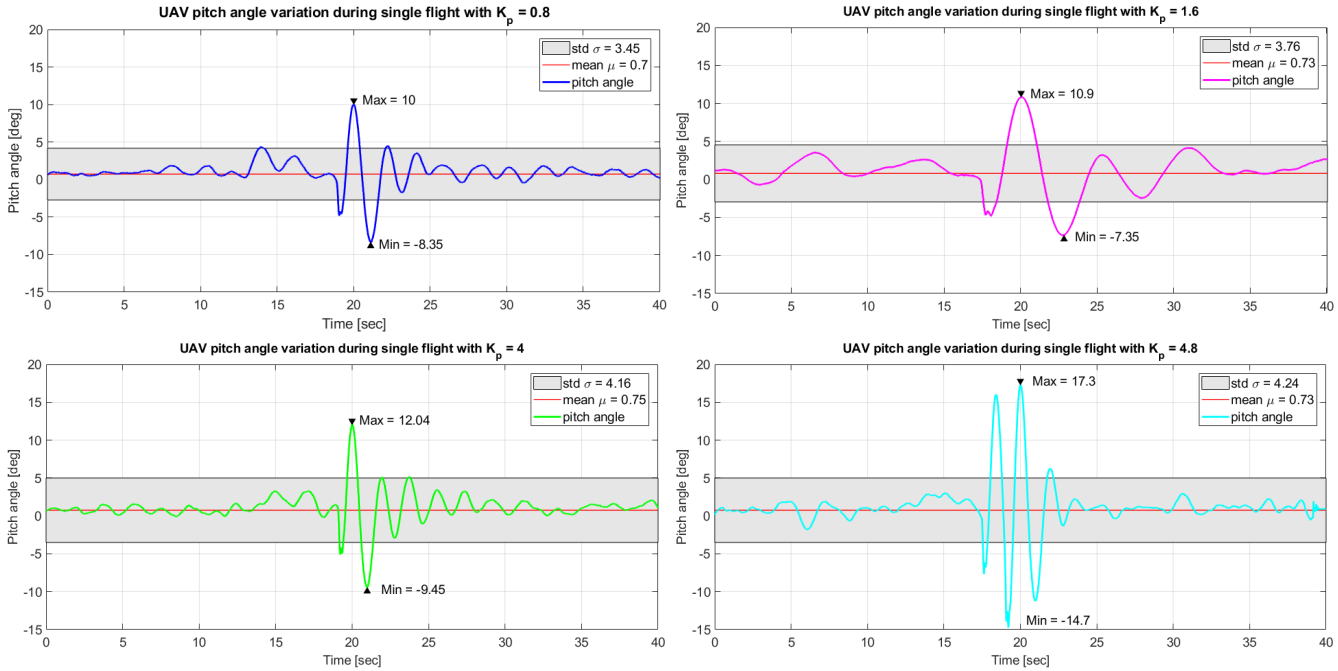

Fig. 4: Four sample flights illustrate the variation in pitch angle over time for each K_p tested. As K_p increases, higher disturbances are sensed in the pitch.

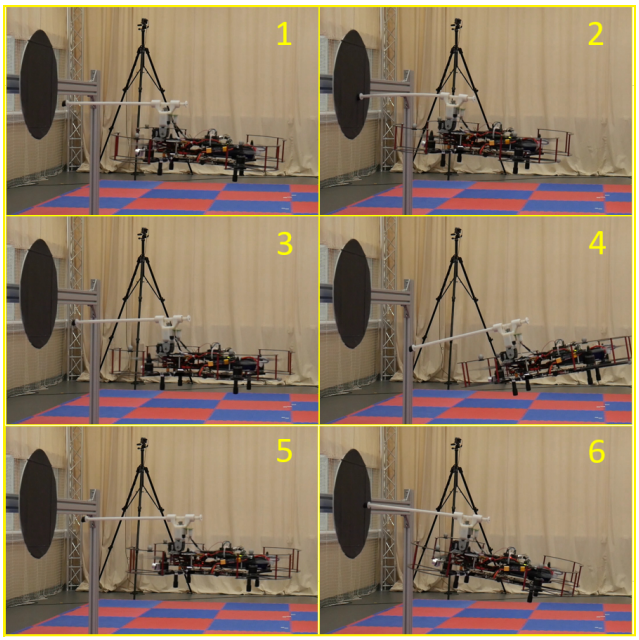

Fig. 5: A time lapse sequence of aerial interaction with a wall, captured during a single flight with K_p = 4.8.

at the end-effector, and this is in line with the theoretical evaluation seen in section II. Figure 7 shows the force exerted with gain $K_p = 4.8$ where a stable interaction is achieved with the wall for a period over 10 seconds. This behaviour is a consequence of the increased PID control action overcoming the static friction of the mechanism and therefore counteracting the wall presence over longer time. A characterisation of the static friction of the system is also presented in fig. 7, where we see how gains smaller than 4.8 (see table I) present a non-linear behaviour until the static friction force $F_{SF} = 18N$ is reached (vertical dashed line). K_p = 4.8 shows a more linear behaviour however, as the gain is high enough to overcome the static friction.

In table III the average of peaks μ_{force}, standard deviation σ_{force} and the maximum force are presented for each K_p. As expected, the mean and maximum values increase with higher gains in the PID, as a stiffer spring is emulated by the controller. The value of σ_{force} in the table provides information on the repeatability of the experiment: higher gains cause an increase in σ up to 4.96 N, as opposed to more compliant configurations that typically provide a more consistent response.

C. Tapping Task

In this section we demonstrate the ability of the proposed manipulator to *tap* onto a surface. The experiment is laid out as follows: the UAV approaches the wall at a constant speed of 0.25 m/sec and, when the wall is in range, the rack protrudes out and establishes contact with it. Then, two setpoints act as lower and upper bounds in the PID control, which periodically switches between them causing the end-effector to tap onto the surface. As a number of sequences is completed, the rack retracts and the UAV is homed.

To validate the tapping behaviour, a set of 10 experiments is conducted at a fixed proportional gain, namely $K_p = 4$.

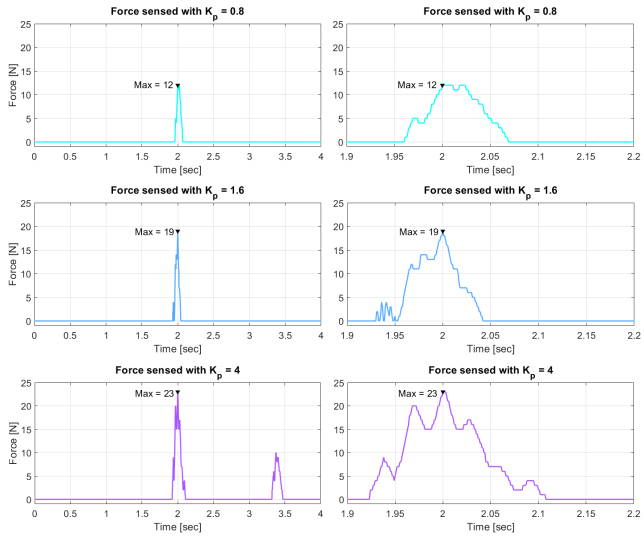

Fig. 6: On the left side - a comparison of forces exerted by the adaptive compliance manipulator for different proportional gains. Lower gains produce a less aggressive behaviour during interaction and therefore lower forces. On the right side - a detailed image of the plots, showing the force curve within [1.9 2.2] seconds.

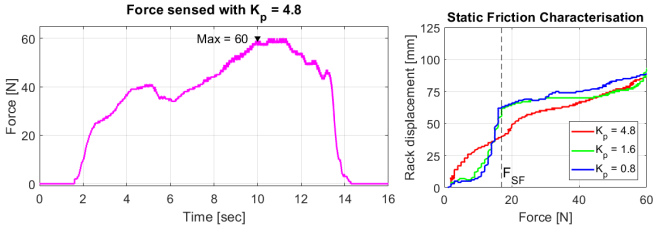

Fig. 7: On the left, the force exerted by the adaptive compliant manipulator during a sample flight with K_p = 4.8. On the right, the characterisation of the static friction of the manipulator.

	K_p = 0.8	K_p = 1.6	K_p = 4	K_p = 4.8
$\mu_{force} \pm \sigma_{force}$	9.66 ±1.86	15 ±2.24	17.5 ±4.11	53.83 ±4.96
max_{force}	12	19	23	60

TABLE III: Average μ and max values of forces sensed whilst pushing and tapping on a surface, with different proportional gains K_p. Each average μ in the table is computed over a number of at least 10 flights for each K_p.

The natural response of the system results in a tapping excitation of approximately 10Hz, as seen in fig. 8. By looking at the force measurement in fig. 8, we identify an initial peak with relatively high force, followed by a period of transition until a steady limit cycle is reached. The average force exerted during tapping throughout all flights is $\mu \pm \sigma = 5.6 \pm 2.27$N, whilst the average frequency response is 11.16Hz. In practice, the desired frequency is application-specific, with typical requirements expected to be in the range of 0-20Hz. Future refinements in both the manipulator and vehicle control system will be focused on minimising the transition period as the aircraft initiates the tapping process, as well as minimising the initial impact and reaching a steady state excitation faster.

V. CONCLUSIONS

The state-of-the-art in aerial physical interaction mostly concerns operations carried out in quasi-static conditions.

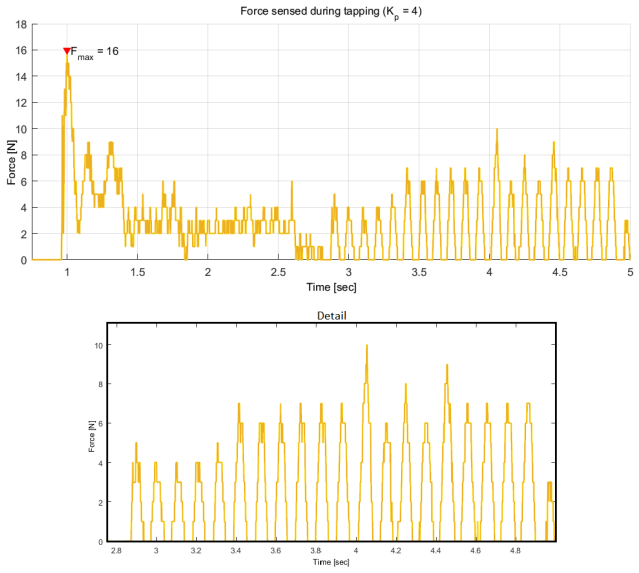

Fig. 8: Tapping force sensed in a sample flight: after an initial impact and transition period the response moves towards a steady limit cycle (displayed in the figure detail).

This study analyses the dynamics resulting from the aerial interaction and derives the relevant design parameters for a manipulation system that is able to exert a range of forces on the environment. It is shown that a manipulator with active compliance is beneficial as it improves the overall aircraft response during an interaction. A compact, adaptively-compliant manipulator is proposed, tailored for both the placement of sensors and the excitation of surfaces. Such type of manipulator is able to adjust the force applied, and generate different behaviours, e.g. provide a regular excitation to a surface over a given period of time.

Based on the experimental findings a refined control model can be formulated and further investigation of its performance will be part of follow-up studies. Future work for this aerial system will include incorporating an adaptive controller for the fine tuning of the manipulator during flight, and the design of an integrated control system that will consider both manipulator and the aircraft as a single, multi-variable system.

REFERENCES

[1] M. Fumagalli, R. Naldi, A. Macchelli, F. Forte, A. Q. Keemink, S. Stramigioli, R. Carloni, and L. Marconi, "Developing an aerial manipulator prototype: Physical interaction with the environment," *Robotics & Automation Magazine, IEEE*, vol. 21, pp. 41–50, 2014.

[2] A. Albers, S. Trautmann, T. Howard, T. A. Nguyen, M. Frietsch, and C. Sauter, "Semi-autonomous flying robot for physical interaction with environment," in *Robotics Automation and Mechatronics (RAM), 2010 IEEE Conference on*, pp. 441–446, IEEE, 2010.

[3] M. Orsag, C. Korpela, and P. Oh, "Modeling and control of mm-uav: Mobile manipulating unmanned aerial vehicle," *Journal of Intelligent & Robotic Systems*, vol. 69, no. 1-4, pp. 227–240, 2013.

[4] M. Orsag, C. Korpela, S. Bogdan, and P. Oh, "Valve turning using a dual-arm aerial manipulator," in *Unmanned Aircraft Systems (ICUAS), 2014 International Conference on*, pp. 836–841, IEEE, 2014.

[5] J. L. Scholten, M. Fumagalli, S. Stramigioli, and R. Carloni, "Interaction control of an uav endowed with a manipulator," in *Robotics and Automation (ICRA), 2013 IEEE International Conference on*, pp. 4910–4915, IEEE, 2013.

[6] M. Ryll, G. Muscio, F. Pierri, E. Cataldi, G. Antonelli, F. Caccavale, and A. Franchi, "6d physical interaction with a fully actuated aerial robot," in *2017 IEEE International Conference on Robotics and Automation*, 2017.

[7] T. Ikeda, S. Yasui, M. Fujihara, K. Ohara, S. Ashizawa, A. Ichikawa, A. Okino, T. Oomichi, and T. Fukuda, "Wall contact by octo-rotor uav with one dof manipulator for bridge inspection," *2017 IEEE/RSJ International Conference on Intelligent Robots and Systems (IROS)*, pp. 5122–5127, 2017.

[8] T. Bartelds, A. Capra, S. Hamaza, S. Stramigioli, and M. Fumagalli, "Compliant aerial manipulators: Toward a new generation of aerial robotic workers," *IEEE Robotics and Automation Letters*, pp. 477–483, Jan 2016.

[9] J. T. Bartelds, "Understanding the critical design parameters of aerial manipulators during physical interaction," msc report 022ram2015, University of Twente, Aug. 2015.

[10] A. Suarez, G. Heredia, and A. Ollero, "Lightweight compliant arm for aerial manipulation," in *Intelligent Robots and Systems (IROS), 2015 IEEE/RSJ International Conference on*, pp. 1627–1632, IEEE, 2015.

[11] A. Suarez, G. Heredia, and A. Ollero, "Lightweight compliant arm with compliant finger for aerial manipulation and inspection," in *Intelligent Robots and Systems (IROS), 2016 IEEE/RSJ International Conference on*, pp. 4449–4454, IEEE, 2016.

[12] S. Hamaza, I. Georgilas, and T. Richardson, "An adaptive-compliance manipulator for contact-based aerial applications," in *2018 IEEE International Conference on Advanced Intelligent Mechatronics (AIM)*, IEEE, 2018, in print.

[13] C. J. Salaan, K. Tadakuma, Y. Okada, E. Takane, K. Ohno, and S. Tadokoro, "Uav with two passive rotating hemispherical shells for physical interaction and power tethering in a complex environment," in *Robotics and Automation (ICRA), 2017 IEEE International Conference on*, pp. 3305–3312, IEEE, 2017.

[14] A. Briod, P. Kornatowski, J.-C. Zufferey, and D. Floreano, "A collision-resilient flying robot," *Journal of Field Robotics*, vol. 31, no. 4, pp. 496–509, 2014.

[15] M. Bisgaard, A. la Cour-Harbo, and J. D. Bendtsen, "Adaptive control system for autonomous helicopter slung load operations," *Control Engineering Practice*, vol. 18, no. 7, pp. 800–811, 2010.

[16] F. Forte, R. Naldi, A. Macchelli, and L. Marconi, "Impedance control of an aerial manipulator," in *American Control Conference (ACC), 2012*, pp. 3839–3844, IEEE, 2012.

[17] G. Giglio and F. Pierri, "Selective compliance control for an unmanned aerial vehicle with a robotic arm," in *Control and Automation (MED), 2014 22nd Mediterranean Conference of*, pp. 1190–1195, IEEE, 2014.

[18] E. Cataldi, G. Muscio, M. A. Trujillo, Y. Rodríguez, F. Pierri, G. Antonelli, F. Caccavale, A. Viguria, S. Chiaverini, and A. Ollero, "Impedance control of an aerial-manipulator: Preliminary results," in *Intelligent Robots and Systems (IROS), 2016 IEEE/RSJ International Conference on*, pp. 3848–3853, IEEE, 2016.

[19] C. Korpela, M. Orsag, M. Pekala, and P. Oh, "Dynamic stability of a mobile manipulating unmanned aerial vehicle," in *Robotics and Automation (ICRA), 2013 IEEE International Conference on*, pp. 4922–4927, IEEE, 2013.

[20] A. Jimenez-Cano, J. Martin, G. Heredia, A. Ollero, and R. Cano, "Control of an aerial robot with multi-link arm for assembly tasks," in *Robotics and Automation (ICRA), 2013 IEEE International Conference on*, pp. 4916–4921, IEEE, 2013.

[21] G. Gioioso, A. Franchi, G. Salvietti, S. Scheggi, and D. Prattichizzo, "The flying hand: A formation of uavs for cooperative aerial tele-manipulation," in *Robotics and Automation (ICRA), 2014 IEEE International Conference on*, pp. 4335–4341, IEEE, 2014.

[22] I. Palunko, P. Cruz, and R. Fierro, "Agile load transportation: Safe and efficient load manipulation with aerial robots," *IEEE Robotics & Automation Magazine*, vol. 19, no. 3, pp. 69–79, 2012.

[23] N. Michael, J. Fink, and V. Kumar, "Cooperative manipulation and transportation with aerial robots," *Autonomous Robots*, vol. 30, no. 1, pp. 73–86, 2011.

[24] D. Mellinger, Q. Lindsey, M. Shomin, and V. Kumar, "Design, modeling, estimation and control for aerial grasping and manipulation," in *Intelligent Robots and Systems (IROS), 2011 IEEE/RSJ International Conference on*, pp. 2668–2673, IEEE, 2011.

[25] P. E. Pounds, D. R. Bersak, and A. M. Dollar, "Grasping from the air: Hovering capture and load stability," in *Robotics and Automation (ICRA), 2011 IEEE International Conference on*, pp. 2491–2498, IEEE, 2011.

[26] J. G. Ziegler and N. B. Nichols, "Optimum settings for automatic controllers," *trans. ASME*, vol. 64, no. 11, 1942.